
Guaranteed confidence-band enclosures for PDE surrogates

Ander Gray
Heudiasyc, UTC

Vignesh Gopakumar
UKAEA & UCL

Sylvain Rousseau
Heudiasyc, UTC

Sébastien Destercke
Heudiasyc, UTC

Abstract

We propose a method for obtaining statistically guaranteed confidence bands for functional machine learning techniques: surrogate models which map between function spaces, motivated by the need build reliable PDE emulators. The method constructs nested confidence sets on a low-dimensional representation (an SVD) of the surrogate model’s prediction error, and then maps these sets to the prediction space using set-propagation techniques. The result are conformal-like coverage guaranteed prediction sets for functional surrogate models. We use zonotopes as basis of the set construction, due to their well studied set-propagation and verification properties. The method is model agnostic and can thus be applied to complex Sci-ML models, including Neural Operators, but also in simpler settings. We also elicit a technique to capture the truncation error of the SVD, ensuring the guarantees of the method.

1 Introduction

One struggles to find an engineering or scientific discipline which has remained untouched from the rapid progression in machine learning (ML) and artificial intelligence (AI). Scientific machine learning (Sci-ML), with tailored architectures for physics-based problems, have in particular driven major advancements. Neural Operators (NOs) (Li et al., 2020), neural networks which can learn between function spaces, have received attention due to their efficient surrogacy of partial differential equation (PDE) solvers (Azizzadenesheli et al., 2024), and have seen application in complex problems including weather modelling (Kurth et al., 2023) and plasma physics (Gopakumar et al., 2024).

However, the wide application of AI methods continues despite widely-shared concerns, as adumbrated by Brundage et al. (2020), Dalrymple et al. (2024), and many others, about the reliability and soundness of these methods. This is an opinion that we share: that methods for AI reliability are underdeveloped in comparison to its progression and wide application.

Although multiple methods exist for uncertainty analysis in AI, little R&D effort has gone into approaches which can provide *quantitative safety guarantees* on the predictions of AI systems. Bayesian machine learning methods, such as Bayesian neural networks, Gaussian processes, Monte Carlo drop-out, and deep ensembles, are powerful methods which can equip predictions with distributional uncertainties. However, they do not attempt to provide statistical *guarantees*. It has also recently been shown by Balch et al. (2019) that Bayesian posteriors (even exact solutions) can suffer from *False Confidence*, meaning that by their nature (additivity) they can produce unsafe results, including in practical/real-world risk calculations, as they demonstrate. Although the advancements in Bayesian machine learning methods has improved AI reliability, for the above reasons alternatives should perhaps be sought for safety-critical systems.

Problem statement Presented with a pre-trained model $\hat{f} : X \mapsto F$, which maps from Euclidean space $X \in \mathbb{R}^m$ to a space of functions $F \in \mathcal{F}$, and some additional (calibration) data unseen by the model $Z = (Z_1, \dots, Z_n)$ where $Z_i = (X_i, F_i)$, construct a prediction set $\mathbb{C}^\alpha \subset \mathcal{F}$ (a band of functions) guaranteed to enclose a next unseen observation F_{n+1} with a user prescribed confidence level: $\mathbb{P}(F_{n+1} \in \mathbb{C}^\alpha) \geq 1 - \alpha$. The space \mathcal{F} has been discretised by a prior analyst $F_1 = [F_1(y_1), \dots, F_1(y_l)] \in \mathbb{R}^l$, but rather finely $l \gg 1$.

1.1 Summary of the method

We briefly outline our strategy.

1. Compute \hat{f} ’s error with respect to the calibration data $e_i = F_i - \hat{f}(X_i)$,
2. Perform a dimension reduction (e.g. an SVD) of e , and project it to a lower dimensional space,

UTC: Université de technologie de Compiègne, UKAEA: UK Atomic Energy Authority, UCL: University College London. Correspondence: Ander.Gray@hds.utc.fr

3. Find an enclosing set \mathcal{Z} of the dimension reduced error, $U_i \in \mathcal{Z}$ for all i , and a point p_Z which is close to the error's mode. In this work we use zonotopes for \mathcal{Z} ,
4. Construct nested confidence regions \mathcal{Z}^α using \mathcal{Z} and p_Z , such that $\mathbb{P}(U_{n+1} \in \mathcal{Z}^\alpha) \geq 1 - \alpha$,
5. Bound truncation error by taking the Cartesian product of the confidence regions \mathcal{Z}^α and a bounding box E of the data of the truncated dimension, $\mathcal{R}^\alpha = \mathcal{Z}^\alpha \times E$,
6. Project \mathcal{R}^α back, and add to the result of the model's prediction $\mathbb{C}^\alpha = \hat{f}(X_{n+1}) + \mathcal{R}^\alpha$.

1.2 Related work

We mention three distinct prior methods for producing guaranteed multivariate prediction sets, however we would not be surprised if there are other methods we have missed, since uncertainty quantification in SciML is quite a timely problem.

Copula-based conformal prediction : [Messouli et al. \(2021\)](#) suggest a method to combine univariate prediction sets obtained from conformal prediction using *copulas*, powerful aggregation functions used to decompose multivariate distributions into their marginals and dependencies. This work was further extended by [Sun and Yu \(2023\)](#) to time series. We note however that using copulas to model dependence in high dimensions is challenging, and their proposition may require more advanced techniques, such as vine-copulas, to be applicable to functional surrogates.

Supremum-based conformal prediction : a quite straightforward way to combine univariate conformal predictors is by taking the supremum over a collection of non-conformity scores. [Diquigiovanni et al. \(2022\)](#) take this idea forward by proposing that the scores of each dimension can be normalised or *modulated* by some function $\sigma(t)$:

$$s(x, y) = \sup_{i \in 1, \dots, N} \left(\sup_{t \in \mathcal{T}} \left| \frac{y_i(t) - \mu(t)}{\sigma(t)} \right| \right),$$

in some prediction region \mathcal{T} of interest, with $\mu(t)$ being the estimated data mean. They suggest that

$$\sigma(t) = \sqrt{\frac{\sum_{i=1}^N (y_i(t) - \mu(t))^2}{N - 1}}$$

is taken to be the estimated data standard deviation. Their method is quite easily adapted to surrogate modelling, by replacing the $\mu(t)$ with a trained predictor $\hat{f}(x_i)(t)$ in both of above expressions, with $\sigma(t)$ now

giving the standard deviation of \hat{f} 's prediction error. Although this method is simple to apply, we find it can at times give quite wide prediction sets.

Elliptical-set conformal prediction : [Messouli et al. \(2022\)](#) propose a multi-target (multivariate) non-conformity score

$$s(x, y) = \sqrt{(y - \hat{f}(x))^\top \hat{\Sigma}^{-1} (y - \hat{f}(x))},$$

where $\hat{\Sigma}$ is sample covariance of the surrogate's prediction error. This non-conformity has a known analytical sublevel-set

$$\mathbb{C}^\alpha = \{y \in \mathbb{R}^n \mid s(x, y) \leq q(\alpha)\},$$

which is an ellipsoid centred at $\hat{f}(x)$, and eccentricity related to $\hat{\Sigma}$. They further show their method extends to 'normalised' conformal prediction, where the ellipsoid changes depending on input x .

1.3 Contributions

Our contribution is most similar to the last of the above methods, where we predict a multivariate set equipped with a guaranteed α -level frequentist performance. Our method diverges as we do not use a non-conformity scoring function, but construct the prediction sets directly on a processed calibration data set.

- A compact representation of probabilistic uncertainty based zonotopes,
- Methods to calibrate this representation from data, forming a probabilistic bound on the unknown training distribution,
- An application of this technique to functional surrogate models, giving guaranteed field enclosures as predictions,
- A method to account for the dimension reduction truncation error, as required by the framework.

2 Conformal prediction and consonant belief functions

In this section we briefly describe inductive conformal prediction, for calibrating guaranteed prediction sets, particularly used for ML models (but not exclusively, as this paper exemplifies), and the related idea of belief functions, which we find to be a useful theory for performing computation using the calibrated sets.

Inductive conformal prediction (ICP) is a computationally efficient version of conformal prediction (Papadopoulos et al., 2002) for computing a set of possible predictions $\mathbb{C}^\alpha : X \mapsto \{\text{subsets of } Y\}$ of an underlying machine learning model $\hat{f} : X \mapsto Y$. The prediction set is equipped with the following probabilistic inequality

$$\mathbb{P}(Y_{n+1} \in \mathbb{C}^\alpha(X_{n+1})) \geq 1 - \alpha. \quad (1)$$

That is, the probability that the next unobserved prediction Y_{n+1} is in computed set $\mathbb{C}^\alpha(X_{n+1})$ is bounded by $1 - \alpha$, where $\alpha \in [0, 1]$ is a user-defined error rate. Additionally, Equation 1 can be *guaranteed* if the data is *exchangeable*, i.e. the data used to build \mathbb{C}^α can be replaced with the future unobserved samples Y_{n+1} without changing their underlying distributions.

Most relevant for this paper is how \mathbb{C}^α is constructed, and how inequality 1 is guaranteed. In ICP, one compares the predictions of a pre-trained model \hat{f} to a *calibration* dataset $Z = (Z_1, Z_2, \dots, Z_n)$ where $Z_i = (X_i, Y_i)$, which is yet unseen by \hat{f} . A non-conformity score $s : X \times Y \mapsto \mathbb{R}$ is used to compare \hat{f} 's predictions to Z_i , with large values of s indicating a large disagreement between the prediction and the ground truth. A common score used in regression is $s(x, y) = |\hat{f}(x) - y|$. When applied to the calibration data $\alpha_i = s(X_i, Y_i)$ gives an ordering of Z_i in terms of how well \hat{f} performs. Moreover, the probability that another (exchangeable) sample $\alpha_{n+1} = s(X_{n+1}, Y_{n+1})$ performs at least as well as previous α_i scores is

$$\mathbb{P}\left(\frac{1}{n} \sum_{i=1}^n \mathbb{I}[\alpha_{n+1} \leq \alpha_i] \leq \epsilon\right) \leq \epsilon, \quad (2)$$

where \mathbb{I} is the indicator function that $\alpha_{n+1} \leq \alpha_i$. Therefore, taking a (conservative) quantile of the sorted scores $q = \alpha_{\lceil (1-\epsilon)n \rceil}$, where $\lceil x \rceil$ denotes the ceiling function, and computing the set of \hat{f} 's possible values giving at least this score $\mathbb{C}^\alpha = \{y \in Y \mid s(x, y) \leq q(\alpha)\}$ gives a set satisfying 1. Note that the prediction regions form a nested family of sets w.r.t α : $\mathbb{C}^{\alpha_1} \supseteq \mathbb{C}^{\alpha_2}$ for $0 \leq \alpha_1 \leq \alpha_2 \leq 1$.

Our framework Computing the level-set of a complicated $s(x, y)$ function may be challenging, so often we opt for quite simple non-conformity scores with known level-sets¹. A challenge which is exacerbated for multivariate problems, somewhat limiting application. We therefore take a different approach, and directly construct \mathbb{C}^α sets using a parametric nested family of sets which we fit to the calibration data (Gupta et al., 2022). This allows us to design prediction sets tailored to our particular data, and well-

suited for multivariate problems. Using an interpretation of \mathbb{C}^α as belief functions, we can perform additional computations (for example linear and non-linear transformations) on \mathbb{C}^α , while still maintaining the guarantee 1. This framework however comes with its own challenges. In some sense we are doing the reverse of conformal prediction, where our challenge is not to compute the level-set $\mathbb{C}^\alpha = \{y \in Y \mid s(x, y) \leq q(\alpha)\}$, rather we begin with \mathbb{C}^α and need to find the membership values $\alpha_i = \sup\{\alpha \in [0, 1] \mid Z_i \in \mathbb{C}^\alpha\}$ of the calibration data. Depending on what set-representation is used, computing the membership values can be a costly operation.

Belief functions Cella and Martin (2022) make a useful connection between conformal prediction and belief functions (Shafer, 1976), a generalisation of the Bayesian theory of probability where one can make set-valued probabilistic statements, such as inequality 1 given by conformal prediction.

Belief functions, also called random-sets or Dempster-Shafer structures, are set-valued random variables whose statistical properties (such their cdf, moments, sample realisations, and probability measure) are set-valued. Belief functions form a bound on a collection of partially unknown random variables, often used in robust risk analysis. In particular, the conformal nested prediction sets \mathbb{C}^α can be related a consonant belief function, and under this framework transformations $f : X \mapsto Y$ of the imprecise random variable are quite simply:

$$\mathbb{C}_Y^\alpha = f(\mathbb{C}_X^\alpha),$$

that is, for each α -level, a single set-propagation of \mathbb{C}_X^α through f is required to determine \mathbb{C}_Y^α , maintaining the same α -confidence level. This is comparatively simpler than other representations, which we use to transform fitted \mathbb{C}_X^α through computations (SVDs in particular).

3 Zonotopic confidence sets

We require a base set-representation to construct the prediction sets \mathbb{C}^α . For this, we chose a class of convex sets known as zonotopes, for some favorable properties, such as being closed under linear transformations and under Minkowski sums. They generalise intervals, boxes, hyper-rectangles, and all their rotations, and may be represented on the computer in a compact manner. An n -dimensional zonotope is completely characterised by a vector in \mathbb{R}^n (centre), and a collection of $p \in \mathbb{N}$ vectors in \mathbb{R}^n (generators).

Definition 1 (Zonotope) Given a centre $c_Z \in \mathbb{R}^n$ and $p \in \mathbb{N}$ generator vectors in a generator matrix

¹E.g., the level set of $|y - \hat{f}(x)|$ is simply $[\hat{f}(x) \pm q]$.

$G_Z = [g_1, \dots, g_p] \in \mathbb{R}^{n \times p}$, a zonotope is defined as

$$\mathcal{Z} = \left\{ x \in \mathbb{R}^n \mid x = c_Z + \sum_{i=1}^p \xi_i g_i, \xi_i \in [-1, 1] \right\}$$

We will use the shorthand notation $\mathcal{Z} = \langle c_Z, G_Z \rangle$.

Zonotopes can equally be characterised as the image of the box $[-1, 1]^p$ by an affine transformation $T(X) = c_Z + G_Z X$. Some example of 2D zonotopes and their generators are shown below (centre is omitted as it corresponds to a translation).

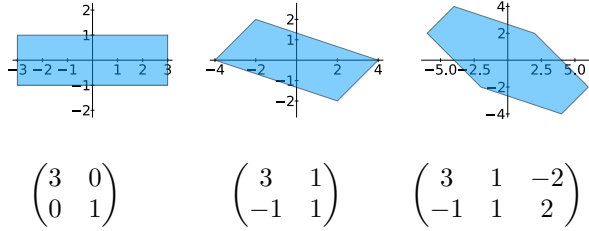


Figure 1: Example zonotopes and their generators.

We will use zonotopes as a basis to construct nested confidence regions, giving the probabilistic guarantee 1, calibrated with respect to a particular dataset. For this, we specify a parametric family of nested zonotopes, parameterised by a value $\alpha \in [0, 1]$. We find that the following parameterisation is simple, and yields nested sets.

Proposition 1 (nested zonotopic sets) *Given a zonotope $\mathcal{Z} = \langle c_Z, G_Z \rangle$, a point $p_Z \in \mathcal{Z}$, the following collection of zonotopes are nested*

$$\mathcal{Z}_{p_Z}^\alpha = \langle c_Z(1 - \alpha) + p_Z\alpha, G_Z(1 - \alpha) \rangle,$$

with $\alpha \in [0, 1]$. $\mathcal{Z}_{p_Z}^\alpha$ are nested in the sense that $\mathcal{Z}_{p_Z}^{\alpha_1} \supseteq \mathcal{Z}_{p_Z}^{\alpha_2}$ for any $\alpha_1 \leq \alpha_2$.

A detailed proof that $\mathcal{Z}_{p_Z}^\alpha$ forms a nested collection of sets is found in appendix A.2. **A quick sketch of the proof** is that we show that the half-spaces $H = \{x \in \mathbb{R}^p \mid a \top x \leq b\}$ composing the box $[-1, 1]^p$ are nested $H^{\alpha_1} \supseteq H^{\alpha_2}$ for $\alpha_1 \leq \alpha_2$ under the transformation $c_Z(1 - \alpha) + p_Z\alpha + G_Z(1 - \alpha)X$.

We also note that $\mathcal{Z}_{p_Z}^{\alpha=0} = \mathcal{Z}$, which can be called the *range* (given it is the largest set in the family), and $\mathcal{Z}_{p_Z}^{\alpha=1} = \{p_Z\}$ (called the *core*). Several examples of parametric nested zonotopes are shown in Figure 2.

Note that the zonotopes $\mathcal{Z}_{p_Z}^\alpha$ are not yet calibrated to anything, so the desired property $\mathbb{P}(X \in \mathcal{Z}_{p_Z}^\alpha) \geq 1 - \alpha$ does not yet hold. The α is so far just a parameter, and needs to be related to a random variable X of interest. In Section 3.2 we explore a method to probabilistically calibrate $\mathcal{Z}_{p_Z}^\alpha$ using conformal prediction. This

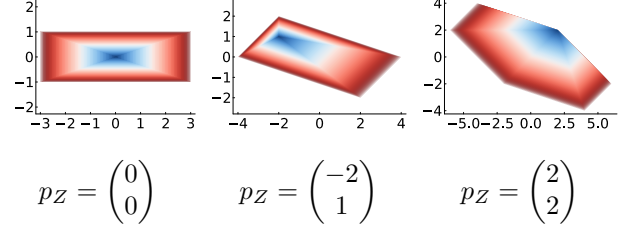


Figure 2: Examples of nested zonotopes families, with \mathcal{Z} from Figure 1 and indicated cores p_Z .

essentially boils down to finding a monotonic function $s : [0, 1] \mapsto [0, 1]$ for α such that the inequality 1 is guaranteed. Indeed, the $\mathcal{Z}_{p_Z}^\alpha$ shown in Figure 2 show a uniformly evaluated α . If one replaces this with a monotonic function $s(\alpha)$, quite dramatically different nested structures are obtained. Examples are shown in Figure 3. One may interpret $s(\alpha)$ as the cumulative probability distribution (cdf) of α , which when sampled yields a random zonotope.

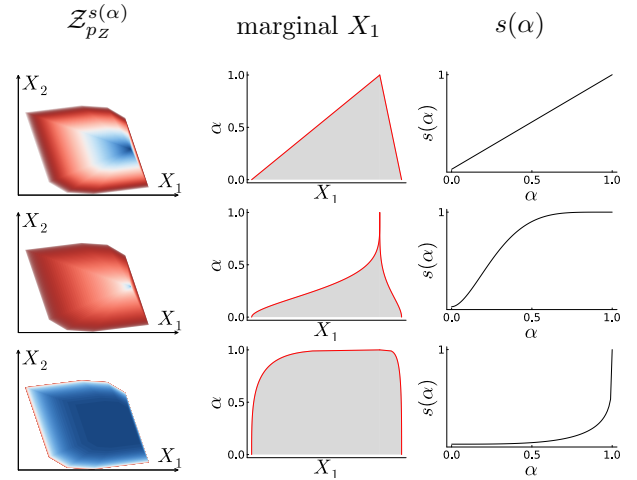


Figure 3: Three examples of the same nested zonotope family $\mathcal{Z}_{p_Z}^\alpha$, but with different $s(\alpha)$ functions. The central column shows the projection of the set onto the X_1 dimension.

We note that inequality 1 can be guaranteed irrespective of the chosen \mathcal{Z} and p_Z , however the ‘quality’ of the confidence sets (their size w.r.t their α confidence-level) depends on how well $\mathcal{Z}_{p_Z}^\alpha$ captures X ’s distribution shape. We therefore require the *shape* of the $\mathcal{Z}_{p_Z}^\alpha$ sets be *fitted* with respect to the dataset. That is given, some data $\{X_1, \dots, X_N\}$ sampled from an unknown distribution $X_i \sim F_X$, we would like to find an enclosing zonotope such that all $X_i \in \mathcal{Z}$. We also require the core p_Z to be fitted, which plays the role of defining the region of the highest confidence, the ‘central’ point of the dataset in some sense. That is,

all the confidence sets will contract towards this point, and so it is desirable for the region around this point to occupy a high density of samples. This point can be determined in terms of *data depth*, how deep a point is in a dataset with respect to some metric. This point is somewhat analogous to the Bayesian posterior mode. Methods to fit $\mathcal{Z}_{p_Z}^\alpha$ are described in Section 3.1.

A potentially interesting corollary of proposition 1 are a simpler family of nested hyperrectangles $\mathcal{B}_{p_B}^\alpha$, in terms of a centre vector $c_B \in \mathbb{R}^n$, radius vector $r_B \in \mathbb{R}^n$, core $p_B \in \mathcal{B}$, and $\alpha \in [0, 1]$.

Corollary 1 *The following family of hyperrectangles are nested*

$$\mathcal{B}_p^\alpha = \left\{ x \in \mathbb{R}^n \mid |x_i - (1 - \alpha)c_i - \alpha p_i| \leq (1 - \alpha)r_i \right\},$$

for all $i = 1, \dots, n$, and with $p \in \mathcal{B}$ and $\alpha \in [0, 1]$.

Some analysis is simpler in terms of hyperrectangles, and so one could opt to use this family rather than $\mathcal{Z}_{p_Z}^\alpha$.

3.1 Fitting zonotopic confidence sets

In this section we discuss various methods to fit $\mathcal{Z}_{p_Z}^\alpha$ to a dataset $X_i \sim F_X$, that is to find a data-enclosing zonotope $X_i \in \mathcal{Z}$ for all samples, and an estimated point p_Z with a high data-depth.

Fitting a rotated hyperrectangle for \mathcal{Z} A simple but effective method is to enclose X_i is using rotated hyperrectangle, with generators G_Z along the principal components of the data.

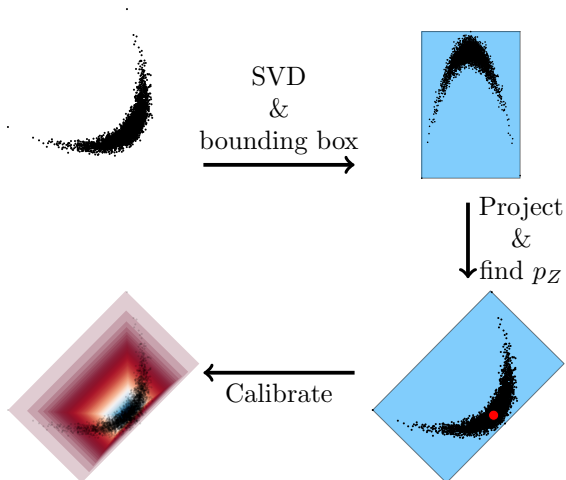


Figure 4: Illustration of fitting a zonotope using the principal components.

A singular value decomposition (SVD) of the data $X = U\Sigma V^\top$ yields a diagonal matrix Σ of (decreasing) singular values and V^\top matrix of singular (or eigen-)

vectors. The singular values provide a natural ranking of the contribution of each eigenvector on the variance of X . An enclosing hyperrectangle can be easily found by computing the data min and max over each dimension of U . Upon converting this hyperrectangle (more details appendix B.1) to a zonotope representation, the zonotope $\mathcal{Z}_U = \langle c_U, G_U \rangle$ can be projected back to the original space by $\mathcal{Z}_X = \langle V\Sigma c_U, V\Sigma G_U \rangle$. This yields a zonotope whose generators are aligned with the eigenvectors of the dataset. Figure 4 illustrates this on a half-moon dataset. Although simple, quick to compute, and scalable, an obvious downside to this method is that it only yields zonotopes with generators as the same number of dimensions of X .

Overapproximating a convex hull for \mathcal{Z} A second method to fit \mathcal{Z} is by first computing the convex hull C_H of X_i , giving a bounding polytope of the data. An enclosing zonotope $\mathcal{Z} \supseteq C_H$ can then be computed (detailed in appendix B.2). This yields a zonotope with half the number of generators as there are bounding half-spaces of C_H . We note that the overapproximation of a convex hull with a zonotope requires a conversion between the vertex representation (v-rep) of polytope to the half-space representation (h-rep), where the v-rep corresponds to a vector of extreme points, and the h-rep is a vector of bounding half-spaces. The conversion from v-rep to h-rep (and vice-versa) can be an expensive operation. Figure 5 illustrates this method on a correlated Gaussian distribution.

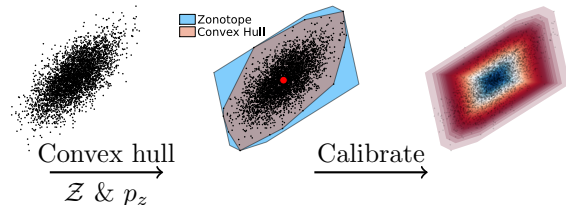


Figure 5: Illustration of fitting using the convex hull.

Additionally, computing C_H can be expensive for higher dimensions or for large quantities of data. For these situations, we recommend the first method, which scales very favorably.

Euclidean data-depth for p_Z A fast and simple, but potentially inaccurate, method is to take p_Z to be the data point X_i with the greatest Euclidean depth w.r.t the sample mean μ

$$p_Z = \arg \max_{X_i} (1 + d_E(X_i))^{-1}$$

where d_E is the Euclidean distance of x to μ

$$d_E(x) = \sqrt{(x - \mu)^\top (x - \mu)}.$$

Mahalanobis data-depth for p_Z A straightforward improvement is to include the data covariance Σ in the depth estimation, using the Mahalanobis distance

$$d_M(x) = \sqrt{(x - \mu)^\top \Sigma^{-1} (x - \mu)},$$

with again p_Z being taken to be the sample X_i with the greatest depth

$$p_Z = \arg \max_{X_i} (1 + d_M(X_i))^{-1}.$$

We find this method also fast, scalable, and more accurate than the Euclidean depth when the data covariance can be inverted. [Messoudi et al. \(2022\)](#) use a metric similar to d_M as a non-conformity score, the level-sets of which are elliptical.

Approximate Tukey's depth for p_Z A popular measure of depth is Tukey's depth (also known as half-space depth), which for a particular point X_i is defined as the smallest number of points from the dataset that can be contained in any half-spaces passing through X_i . I.e. what is the smallest data partition that can be obtained

$$d_T(x) = \inf_{v \in \mathbb{R}^d} \frac{1}{n} \sum_{j=1}^n \mathbb{I}\{v^\top (X_j - x) \geq 0\},$$

where \mathbb{I} is the indicator function that the sample X_i is in the half-space defined by vector v and point x . We then pick p_Z to be the point with the greatest depth

$$p_Z = \arg \max_{X_i} d_T(X_i).$$

Although Tukey's depth is robust, it is highly expensive to compute (requiring 2 loops over the data), we therefore find this approximate Tukey's depth performs quite well up to moderate dimensions

$$\tilde{d}_T(x) = \inf_{v \in V} \frac{1}{n} \sum_{j=1}^n \mathbb{I}\{v^\top (X_j - x) \geq 0\},$$

where V are the normal vectors of the data enclosing set. That is, one only checks the half-spaces composing the enclosing zonotope \mathcal{Z} .

3.2 Calibrating zonotopic confidence sets

Calibration with a known distribution For mostly illustrative purposes, we begin by showing how $\mathcal{Z}_{p_Z}^\alpha$ can be calibrated from a known multivariate distribution, whose cdf F_X or density f_X are available. This could perhaps be useful for some applications, but the next method (calibrating from sample data) is likely to find wider use. Given a zonotope \mathcal{Z} , ideally

containing the range of f_X or otherwise some large probability region ($\mathbb{P}_X(\mathcal{Z}) \approx 1$) if X is unbounded, and a p_Z ideally near the mode, the structure can be calibrated by integrating the density f_X in the sets $\mathcal{Z}_{p_Z}^\alpha$:

$$s(\alpha) = 1 - \int_{\mathcal{Z}_{p_Z}^\alpha} f_X(x) dx.$$

The condition

$$\mathbb{P}(X \in \mathcal{Z}_{p_Z}^{s(\alpha)}) \geq 1 - \alpha$$

holds straightaway.

Calibration from sample data Our method is similar to conformal prediction, as described in section 2, however without a trained regressor \hat{f} and our data $\{X_1, X_2, \dots, X_n\}$ is multidimensional. We also have a parametric set family $\mathcal{Z}_{p_Z}^\alpha$ in contrast to a non-conformity scoring function. However, the set-membership of the data $\alpha_i = \sup\{\alpha \in [0, 1] \mid X_i \in \mathcal{Z}_{p_Z}^\alpha\}$ can be used to rank or score the data. Under the assumption of exchangeability, the probability of another X_{n+1} having a membership score as extreme as the α_i 's is equation 2. This directly leads to the (conservative) quantile $s(\epsilon) = \alpha_{[\epsilon n]}$ with sorted α producing a set with the property

$$\mathbb{P}(X_{n+1} \in \mathcal{Z}_{p_Z}^{s(\epsilon)}) \geq 1 - \epsilon, \quad (3)$$

where $\epsilon \in [0, 1]$ is a user defined confidence value.

We note that computing the exact membership score $\alpha_i = \sup\{\alpha \in [0, 1] \mid X_i \in \mathcal{Z}_{p_Z}^\alpha\}$ may be challenging, as the set must be varied with α until $X_i \notin \mathcal{Z}_{p_Z}^\alpha$, which could be relatively well performed using mathematical optimisation for certain set representations. We however suggest a simple method, where α uniformly discretised in a grid in $A = \{0, 0.111, \dots, 0.999, 1\}$, and computing

$$\alpha_i = \max\{\alpha \in A \mid X_i \in \mathcal{Z}_{p_Z}^\alpha\}. \quad (4)$$

Although the exact supremum isn't found, this still gives conservative results, as two collection of scores $\alpha_i \leq \alpha_j$ will yield a lower bound on probabilistic bound on 3. I.e. larger confidence set $\mathcal{Z}_{p_Z}^{\alpha_i} \supseteq \mathcal{Z}_{p_Z}^{\alpha_j}$. We suggested that the discretisation of the α values is as least as large as the data set, to avoid multiple repetitions of the same α_i values as much as possible. Also note that like in conformal prediction, the maximum number of unique prediction sets that can be obtained is the number of calibration data points provided. Figure 6 gives three examples of calibrating $\mathcal{Z}_{p_Z}^\alpha$ using this method with different data lengths.

Some potential alternative frameworks exist for reliably calibrating $\mathcal{Z}_{p_Z}^\alpha$, including inferential models

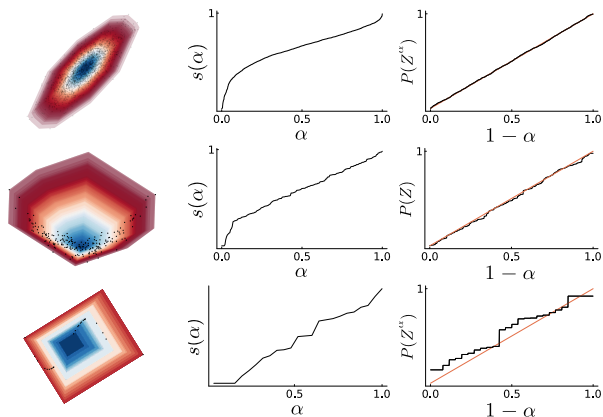


Figure 6: Shows three examples of calibration using conformal prediction. The top row shows a correlated Gaussian of 2000 points, and the middle a 200 samples of a skewed half-moon, and bottom 25 samples of a sin function. The final column shows the empirically tested coverage.

(Martin and Liu, 2015), confidence-structures (Balch, 2012), frequency-calibrated belief functions (Dencoux and Li, 2018), and scenario theory (De Angelis et al., 2021). There are likely strong links between these methods and what is proposed here.

4 Functional confidence-bands

Given a pre-trained model $\hat{f} : X \mapsto F$, which maps from Euclidean space $X \in \mathbb{R}^m$ (space of PDE inputs) to a space of functions $F \in \mathcal{F}$ (PDE solutions), discretised on a fine grid $F_1 = [F_1(y_1), \dots, F_1(y_l)] \in \mathbb{R}^l$, we can compute the error of \hat{f} 's error on some unseen data $\{(X_1, F_1), \dots, (X_n, F_n)\}$ with $e_i = F_i - \hat{f}(X_i)$. We may then reduce the dimension of e_i using an SVD: $e = U\Sigma V^\top$, where the singular values indicate the variance contribution of each eigenvector to the variance of e_i . We may truncate the dimensions of the data, capturing some high (often 99%) of the overall variance, and projecting the data e_i onto these remaining dimensions, a low dimension representation of \hat{f} 's error: U_i . Depending on the size of these dimensions, one of the above fitting methods may be applied to find \mathcal{Z}_{pz}^α . We find the 'rotated hyperrectangle' method and the Mahalanobis depth scale well to high dimensions, with the convex hull method being tighter for smaller dimensions. \mathcal{Z}_{pz}^α may then be calibrated, giving $\mathbb{P}(U_{n+1} \in \mathcal{Z}^\alpha) \geq 1 - \alpha$. Mapping \mathcal{Z}_{pz}^α through the linear transformation back to \mathbb{R}^l is straightforward for the underlying zonotope, and for the probabilistic part α , propagate each zonotope level-set independently $\mathcal{R}^\alpha = f(\mathcal{Z}_{pz}^\alpha)$, i.e. perform one transformation for each confidence-level, with the α -guaranteed being retained by the set. Note we may perform this since we

compute a multivariate confidence set, this would not be the case had each dimension been fit independently.

These nested sets can be added to the prediction of \hat{f} , yielding the desired functional prediction set

$$\mathbb{C}_F^\alpha = \hat{f}(X_{n+1}) + \mathcal{R}^\alpha.$$

However, the resulting confidence regions are not strictly a guaranteed bound on (X_{n+1}, F_{n+1}) , since we have truncated some data variance during the fitting. Although these dimensions weakly effect the variance of F_i , we cannot strictly claim a guaranteed bound. We therefore propose a quite simple method to account for the uncertainty in these dimensions, without including them in the expensive set calibration.

4.1 Bounding truncation error

By taking a bounding box of F_i 's projection onto the truncated eigenvectors, one can obtain an estimate of the range of uncertainty in these dimensions, that is, the range of \mathcal{Z} had we included these dimensions. We capture this error with a simple bounding hyperrectangle E found using the data minimum and maximum in each dimension. Upon taking the Cartesian product $\mathcal{R}^\alpha = \mathcal{Z}_{pz}^\alpha \times E$, one obtains a zonotope in high dimensions which contracts in the important directions as α varies, but remains constant in the truncated dimensions. The α -guarantee remains unchanged due to this operation because: 1) the number of data points remains unchanged (only their dimension), and 2) the data is totally bounded (and remains so as α changes) in the extra dimensions. Indeed, there is a slight performance-loss when performing this (our probabilistic bound becomes looser), however this is quite minor as these extra dimensions don't affect F_i dramatically. The Cartesian product between two zonotopes $\mathcal{Z}_X \subset \mathbb{R}^n$ and $\mathcal{Z}_Y \subset \mathbb{R}^m$ produces an additional zonotope $\mathcal{Z}_{X \times Y} \subset \mathbb{R}^{n \times m}$, whose centre and generator are a simple concatenation of the centres and generators of \mathcal{Z}_X and \mathcal{Z}_Y : $c_{X \times Y} = (c_X || c_Y)$ and $G_{X \times Y} = (G_X || G_Y)$.

4.2 PDE surrogate example

We use `LazySets.jl` from Forets and Schilling (2021) for the set construction, and `NeuralOperators.jl` for the base Sci-ML model. Otherwise, a supplementary code repository will be released for those wishing to reproduce this papers results.

To demonstrate the methodology, we construct functional confidence bands on a Fourier neural operator (FNO) for the Burger's equation, trained on data supplementary data provided from Li et al. (2020), which was built by sampling a numerical PDE solver.

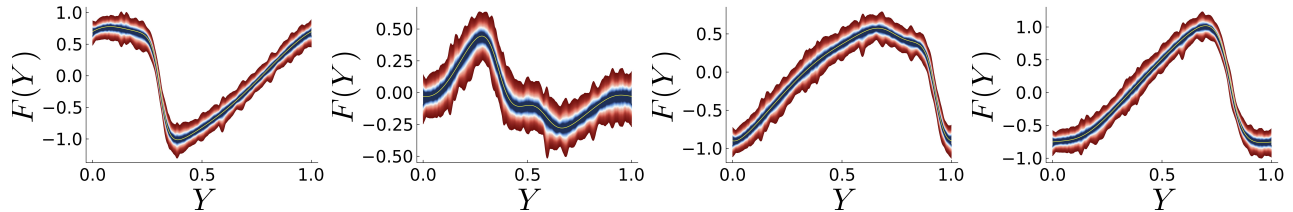


Figure 7: Examples of constructed confidence-bands of the FNO for Burger’s equation, predicted on test data set. The ground truth is shown in yellow.

The FNO model was trained on an A100 GPU using `NeuralOperators.jl`, using 2048 points to train the underlying model, 1000 point for calibrating the confidence bands, and 1048. Additional information about the training setup, and about the underlying PDEs, can be found in appendix C. The predictions from the FNO are discretise onto a grid of 1024 points. A 32-dimensional rotated hyperrectangle was fitted on the important directions the error’s SVD, with p_Z found using the Mahalanobis depth. The entire calibration process took 75s on a modern laptop, with most of the computation spent on computing the membership 4 of the calibration data. Once calibrated, computing a prediction is timed at 0.02s. Four realisations of the training dataset are shown in Figure 7, with the ground truth shown in yellow.

We also note that a 1024 nested zonotopic set is predicted for the output of the FNO, what’s shown in Figure 7 is the axis projection of this set. If we inspect the individual axis, the dependence of the field can also be seen captured.

5 Relationships to other ideas

5.1 Non-convex confidence sets

It is fairly straightforward to extend the above to other set-representations, for example Taylor-models or polynomial zonotopes, with examples shown in Figure 8. However, a compact representation, like our proposition 1 is challenging for more complex set representations. The below sets were constructed by first constructing a $\mathcal{Z}_{p_Z}^\alpha \subseteq [-1, 1]^p$, and mapping this through the corresponding Taylor polynomial. Although this allows us to compute level-sets (and therefore memberships 4), an efficient method to fit these sets to data would need to be proposed.

This more sophisticated set-representation could allow us to perform a more aggressive non-linear dimension reduction. A potentially interesting application of this work would be to probabilistically fit from data the set-representations used in dynamical system verification.

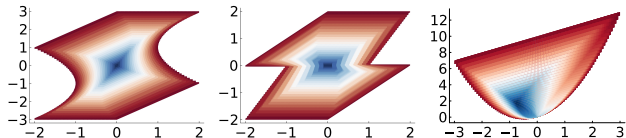


Figure 8: Example nested polynomial zonotopes.

5.2 Relationship to conformal prediction

The proposed method is similar to conformal prediction, but where we directly solve for a valid prediction set, instead of taking a level-set of a non-conformity scoring function. Indeed, the membership function of $\mathcal{Z}_{p_Z}^\alpha$ is the non-conformity score in conformal prediction. If one could find an efficient (perhaps analytical) expression for this membership function, in terms of α and the underlying set-representation, then the calibration procedure would be made much more efficient (corresponding to a simple function evaluation), without the need to check the set-membership of $\mathcal{Z}_{p_Z}^\alpha$ in 4, which is a costly part of the proposition. This would also additionally greatly simplify the implementation.

We therefore share many of the advantages and disadvantages of conformal prediction, including finite-sample guarantees and being model agnostic. Although we show example of regression problems, we believe our method could apply to multivariate classification problems.

6 Limitations

Our method requires the same assumption as conformal prediction, namely exchangeability, we therefore suffer similar limitations. The guarantee is lost if the dataset is not exchangeable (for example if it changes over time). We also give only marginal coverage (averaged for all samples of X_i), rather than the stronger conditional coverage (conditioned for particular x), which is more desirable for surrogate modelling. Finally, we mention that our method would greatly benefit for refined methods for fitting set-representations to data. Although the routines we proposed are simple, we do not doubt that more sophisticated methods

can be found, to improve the tightness of the fitted set.

Acknowledgements

This project was provided with HPC and AI computing resources and storage by GENCI at IDRIS thanks to the grant 2024-AD010615449 on the *Jean Zay* supercomputer's CSL, V100 and A100 partitions.

References

- K. Azizzadenesheli, N. Kovachki, Z. Li, M. Liu-Schiaffini, J. Kossafi, and A. Anandkumar. Neural operators for accelerating scientific simulations and design. *Nature Reviews Physics*, pages 1–9, 2024.
- M. S. Balch. Mathematical foundations for a theory of confidence structures. *International Journal of Approximate Reasoning*, 53(7):1003–1019, 2012.
- M. S. Balch, R. Martin, and S. Ferson. Satellite conjunction analysis and the false confidence theorem. *Proceedings of the Royal Society A*, 475(2227):20180565, 2019.
- M. Brundage, S. Avin, J. Wang, H. Belfield, G. Krueger, G. Hadfield, H. Khlaaf, J. Yang, H. Toner, R. Fong, et al. Toward Trustworthy AI Development: Mechanisms for Supporting Verifiable Claims, 2020. URL <https://arxiv.org/abs/2004.07213>.
- L. Cella and R. Martin. Validity, consonant plausibility measures, and conformal prediction. *International Journal of Approximate Reasoning*, 141:110–130, 2022.
- D. Dalrymple, J. Skalse, Y. Bengio, S. Russell, M. Tegmark, S. Seshia, S. Omohundro, C. Szegedy, B. Goldhaber, N. Ammann, et al. Towards Guaranteed Safe AI: A Framework for Ensuring Robust and Reliable AI Systems. *arXiv preprint arXiv:2405.06624*, 2024.
- M. De Angelis, R. Rocchetta, A. Gray, and S. Ferson. Constructing consonant predictive beliefs from data with scenario theory. In *International Symposium on Imprecise Probability: Theories and Applications*, pages 357–360. PMLR, 2021.
- T. Denceux and S. Li. Frequency-calibrated belief functions: review and new insights. *International Journal of Approximate Reasoning*, 92:232–254, 2018.
- J. Diquigiovanni, M. Fontana, and S. Vantini. Conformal prediction bands for multivariate functional data. *Journal of Multivariate Analysis*, 189:104879, 2022.
- M. Forets and C. Schilling. LazySets.jl: Scalable Symbolic-Numeric Set Computations. *Proceedings of the JuliaCon Conferences*, 1(1):11, 2021. doi: 10.21105/jcon.00097.
- V. Gopakumar, S. Pamela, L. Zanisi, Z. Li, A. Gray, D. Brennand, N. Bhatia, G. Stathopoulos, M. Kusner, M. P. Deisenroth, et al. Plasma surrogate modelling using Fourier neural operators. *Nuclear Fusion*, 64(5):056025, 2024.
- C. Gupta, A. K. Kuchibhotla, and A. Ramdas. Nested conformal prediction and quantile out-of-bag ensemble methods. *Pattern Recognition*, 127:108496, 2022. ISSN 0031-3203. doi: <https://doi.org/10.1016/j.patcog.2021.108496>. URL <https://www.sciencedirect.com/science/article/pii/S0031320321006725>.
- T. Kurth, S. Subramanian, P. Harrington, J. Pathak, M. Mardani, D. Hall, A. Miele, K. Kashinath, and A. Anandkumar. Fourcastnet: Accelerating global high-resolution weather forecasting using adaptive Fourier neural operators. In *Proceedings of the platform for advanced scientific computing conference*, pages 1–11, 2023.
- Z. Li, N. Kovachki, K. Azizzadenesheli, B. Liu, K. Bhattacharya, A. Stuart, and A. Anandkumar. Fourier neural operator for parametric partial differential equations. *arXiv preprint arXiv:2010.08895*, 2020.
- R. Martin and C. Liu. *Inferential models: reasoning with uncertainty*. CRC Press, 2015.
- S. Messoudi, S. Destercke, and S. Rousseau. Copula-based conformal prediction for multi-target regression. *Pattern Recognition*, 120:108101, 2021.
- S. Messoudi, S. Destercke, and S. Rousseau. Ellipsoidal conformal inference for multi-target regression. In *Conformal and Probabilistic Prediction with Applications*, pages 294–306. PMLR, 2022.
- H. Papadopoulos, K. Proedrou, V. Vovk, and A. Gammerman. Inductive confidence machines for regression. In *Machine learning: ECML 2002: 13th European conference on machine learning Helsinki, Finland, August 19–23, 2002 proceedings 13*, pages 345–356. Springer, 2002.
- G. Shafer. *A mathematical theory of evidence*, volume 42. Princeton university press, 1976.
- S. H. Sun and R. Yu. Copula conformal prediction for multi-step time series prediction. In *The Twelfth International Conference on Learning Representations*, 2023.

Appendix for “Guaranteed confidence-band enclosures for PDE surrogates”

A Further detail about proposition 1.

Here we provide additional detail about the proposed nested zonotope family $\mathcal{Z}_{p_Z}^\alpha$, and a proof that the family is a nested.

A.1 Intuition behind the nested family

Figure 9 gives a visual description of how the nested sets $\mathcal{Z}_{p_Z}^\alpha$ are constructed. Given a zonotope \mathcal{Z} and a point $p_Z \in \mathcal{Z}$, the centres of the parametric zonotopes move along the line defined by $c_Z(1 - \alpha) + p_Z\alpha$, and additionally the generators are contracted by $(1 - \alpha)$. Thus, the zonotopes are translated toward p_Z as α increases, and their size reduces. Figure 9 shows an example of a parametric zonotope being constructed for $\alpha = 0.5$. Note that all the sets in $\mathcal{Z}_{p_Z}^\alpha$ have the same shape, and only differ by a translation and a contraction. This is partially because all generators are scaled by the same magnitude. Note: c_Z does not need to be inside all zonotopes, however the point p_Z is inside all zonotopes. Indeed, it is the *only* point that is in all zonotopes (given $\mathcal{Z}_{p_Z}^{\alpha=1} = \{p_Z\}$).

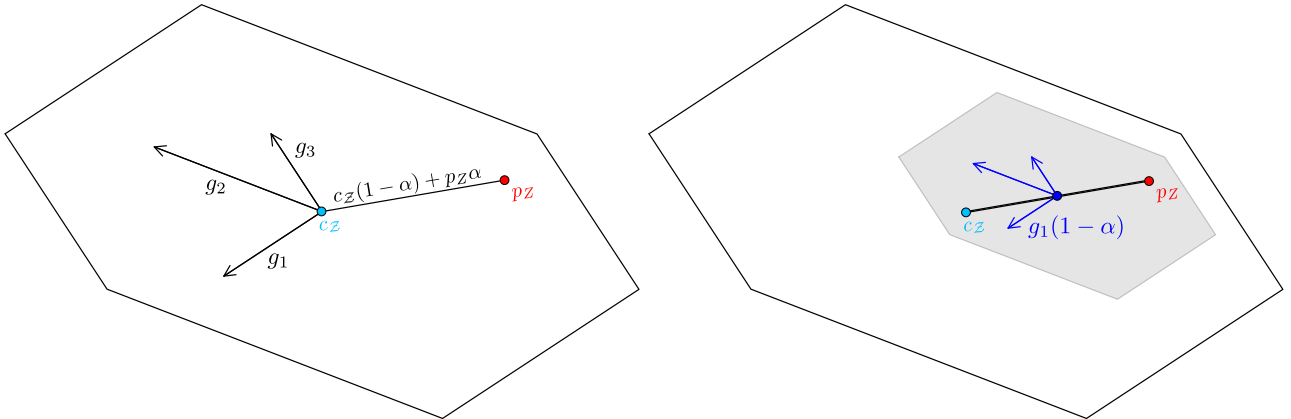


Figure 9: (Left) Shows the outline of an example \mathcal{Z} , with generators plotted. Zonotope centre c_Z is in cyan and core p_Z in red, and shows the parametric line defined by $c_Z(1 - \alpha) + p_Z\alpha$. (Right) Same outline of \mathcal{Z} , additionally with the zonotope defined at $\alpha = 0.5$ in grey, which has its centre halfway in between c_Z and p_Z , and its generators scaled by 0.5.

A.2 Proof of proposition 1.

Here we provide a detailed proof of proposition 1. (nested zonotopic sets), that $\mathcal{Z}_{p_Z}^{\alpha_1} \supseteq \mathcal{Z}_{p_Z}^{\alpha_2}$ for any $0 \leq \alpha_1 \leq \alpha_2 \leq 1$. We remind you that $\mathcal{Z}_{p_Z}^\alpha$ is defined as

$$\mathcal{Z}_{p_Z}^\alpha = \left\{ x \in \mathbb{R}^n \mid x = c_Z(1 - \alpha) + p_Z\alpha + \sum_{i=1}^p \xi_i g_i(1 - \alpha), \quad \xi_i \in [-1, 1] \right\},$$

for some point $p_Z \in \mathcal{Z}$ and $\alpha \in [0, 1]$. The proof is based on the following rational:

1. Take two sets L and K composed as the intersection of n sets $L = \bigcap_{i=1}^n A_i$ and $K = \bigcap_{i=1}^n B_i$, if each $B_i \subseteq A_i$, then $K \subseteq L$.

2. Since a zonotope can be considered as an intersection of half-spaces (H-representation), it suffices to study the subset-hood of the individual half-spaces composing $\mathcal{Z}_{p_z}^{\alpha_1}$ and $\mathcal{Z}_{p_z}^{\alpha_2}$.
3. A zonotope $\mathcal{Z} = \langle c_{\mathcal{Z}}, G_{\mathcal{Z}} \rangle$ can be characterised as the image of the box $\times_1^n[-1, 1]$ in \mathbb{R}^n , where n is the number generators, by an affine transformation defined by the rotation and stretching with matrix $G_{\mathcal{Z}}$ and translation with vector $c_{\mathcal{Z}}$.
4. Equivalently it can be defined as the intersection of the same affine transformation of the half-spaces defining the box $\times_1^n[-1, 1]$.
5. A half-space $H_1 = \{x \in \mathbb{R}^n | a_1^\top x \leq b_1\}$ is a subset of another half-space $H_2 = \{x \in \mathbb{R}^n | a_2^\top x \leq b_2\}$, $H_1 \subseteq H_2$ if:
 - (a) a_1 and a_2 are positively aligned, i.e., they are parallel and have the same direction: $a_1 \leq \lambda a_2$ for $\lambda \geq 0$.
 - (b) $b_1 \leq \lambda b_2$, where λ the same as (a).

Condition (a) is straightforward to prove: $\mathcal{Z}_{p_z}^{\alpha_1}$ transforms any half-space normal vectors a as

$$(G_{\mathcal{Z}}(1 - \alpha_1))^{-\top} a = (1 - \alpha_1)^{-1} G_{\mathcal{Z}}^{-\top} a = (1 - \alpha_1)^{-1} a',$$

and $\mathcal{Z}_{p_z}^{\alpha_2}$ as

$$(G_{\mathcal{Z}}(1 - \alpha_2))^{-\top} a = (1 - \alpha_2)^{-1} G_{\mathcal{Z}}^{-\top} a = (1 - \alpha_2)^{-1} a'.$$

Therefore, since $\alpha_1 \leq \alpha_2$:

$$(1 - \alpha_1)^{-1} a' \leq (1 - \alpha_2)^{-1} a',$$

holds, and therefore half-spaces transformed by $\mathcal{Z}_{p_z}^{\alpha_1}$ and $\mathcal{Z}_{p_z}^{\alpha_2}$ are parallel and have the same direction. We additionally know that the normal vector a' is contracted by $\lambda = (1 - \alpha_2)/(1 - \alpha_1)$ and that $\lambda \in [0, 1]$. For condition (b), $\mathcal{Z}_{p_z}^{\alpha_1}$ transforms any half-space offset b as

$$\begin{aligned} b_1 &= b + a^\top (G_{\mathcal{Z}}(1 - \alpha_1))^{-1} (c_{\mathcal{Z}}(1 - \alpha_1) + p_z \alpha_1) \\ &= b + (1 - \alpha_1)^{-1} a^\top (G_{\mathcal{Z}}^{-1} c_{\mathcal{Z}}(1 - \alpha_1) + G_{\mathcal{Z}}^{-1} p_z \alpha_1). \end{aligned}$$

Setting $J_{\mathcal{Z}} = G_{\mathcal{Z}}^{-1} c_{\mathcal{Z}}$ and $K_{\mathcal{Z}} = G_{\mathcal{Z}}^{-1} p_z$:

$$\begin{aligned} b_1 &= b + (1 - \alpha_1)^{-1} a^\top (J_{\mathcal{Z}}(1 - \alpha_1) + K_{\mathcal{Z}} \alpha_1) \\ &= b + a^\top (J_{\mathcal{Z}} + \alpha_1 (1 - \alpha_1)^{-1} K_{\mathcal{Z}}) \\ &= b + a^\top J_{\mathcal{Z}} + \alpha_1 (1 - \alpha_1)^{-1} a^\top K_{\mathcal{Z}}. \end{aligned}$$

By symmetry, we also know that for $\mathcal{Z}_{p_z}^{\alpha_2}$:

$$b_2 = b + a^\top J_{\mathcal{Z}} + \alpha_2 (1 - \alpha_2)^{-1} a^\top K_{\mathcal{Z}}.$$

Inserting these two expressions into our inequality $b_1 \leq (1 - \alpha_2)/(1 - \alpha_1) b_2$ and simplifying (noting that $a^\top J_{\mathcal{Z}}$ and $a^\top K_{\mathcal{Z}}$ are scalar):

$$\begin{aligned} \alpha_1 (1 - \alpha_1)^{-1} &\leq (1 - \alpha_2)/(1 - \alpha_1) \alpha_2 (1 - \alpha_2)^{-1} \\ \alpha_1 &\leq \alpha_2. \end{aligned}$$

Thus, any half-space H transformed by $\mathcal{Z}_{p_z}^{\alpha}$ has the property $H^{\alpha_1} \supseteq H^{\alpha_2}$ for any $\alpha_1 \leq \alpha_2$, and $\mathcal{Z}_{p_z}^{\alpha_1} \supseteq \mathcal{Z}_{p_z}^{\alpha_2}$ for any $\alpha_1 \leq \alpha_2$, concluding the proof.

B Relationships between set-representations used in the paper

We find the `LazySets.jl`² (Forets and Schilling, 2021) manual, and software docstrings, quite thorough resources for set-representations and their respective overapproximations. Here we summarise some set isomorphisms and overapproximations used the main paper.

²<https://github.com/JuliaReach/LazySets.jl>

B.1 Converting hyperrectangles to zonotopes

Hyperrectangles are exactly representable as zonotopes. A hyperrectangle $\mathcal{B} \subset \mathbb{R}^n$ with centre vector $C_{\mathcal{B}} \in \mathbb{R}^n$ and radius vector $R_{\mathcal{B}} \in \mathbb{R}^n$, has the same centre in zonotopic representation $C_{\mathcal{Z}} = C_{\mathcal{B}}$, and a diagonal generator matrix $G_{\mathcal{Z}} \in \mathbb{R}^{n \times n}$ with the radius vector along the diagonals $G_{\mathcal{Z}} = I_n R_{\mathcal{B}}$, where I_n is the identity matrix in n dimensions.

B.2 Overapproximating a polytope with a zonotope

With the algorithm initially proposed by Guibas et al. (2003) (section 4.2), here we summarise the version implemented in LazySets.jl (Forets and Schilling, 2021). Further detail can be found therein.

Given a polytope C_H in vertex representation (for example the result of a convex hull of a dataset) with vertices v_k , and some user-selected directions d_k (to which the constructed zonotope’s generators will be parallel to), the overapproximation $\mathcal{Z} \supseteq C_H$ can be performed by solving the following linear program:

$$\begin{aligned} & \min \sum_{k=1}^l \alpha_k \\ & \text{s.t.} \\ & v_j = c + \sum_{k=1}^l b_{kj} d_k \quad \forall j \\ & -\alpha_k \leq b_{kj} \leq \alpha_k \quad \forall k, j \\ & \alpha_k \geq 0 \quad \forall k. \end{aligned}$$

The resulting zonotope has center c and generators $\alpha_k d_k$. In this work, we take the directions d_k to be the normal vectors of the enclosing half-spaces the initial polytope.

C Fourier Neural Operators, Burgers’ equation, and Training

Here we provide extra details about the example PDE, the functional surrogate model, and its training, used in the main paper.

C.1 Burgers’ Equation

The Burgers’ equation is a partial differential equation often used to model the convection-diffusion of a fluid, gas, or non-linear acoustics. The one-dimensional equation is

$$\frac{\partial u}{\partial t} + u \frac{\partial u}{\partial y} = \nu \frac{\partial^2 u}{\partial^2 y},$$

where u defines the field variables, ν the kinematic viscosity, and with y and t being the spatial and temporal coordinates respectively. We define a family of initial conditions as follows:

$$u(y, t = 0) = \sin(\alpha\pi y) + \cos(-\beta\pi y) + \frac{1}{\cosh(\gamma\pi y)},$$

parameterised by $\alpha \in [-3, 3]$, $\beta \in [-3, 3]$, and $\gamma \in [-3, 3]$.

Data set generation A dataset of 2048 (training) + 1000 (calibration) + 1048 (validation) PDE solutions is generated by Latin Hypercube sampling (uniform) the α , β , and γ parameters (thus generating random initial conditions for the PDE), and then solving Burgers’ equation using a spectral solver (Canuto, 2007). Each simulation is run for 500-time iterations with a $\Delta t = 0.0025$ time step and a spatial domain spanning $[0, 1]$, uniformly discretised into 1024 spatial units. The field at the last time point is then saved as the output, and the surrogate’s task is to learn the mapping from the initial condition to the fields final state $u(y, 0) \rightarrow u(y, t_{\text{end}})$.

C.2 Fourier Neural Operators

Fourier Neural Operators (FNOs), introduced by Li et al. (2020), are specific instance of the Neural Operator (NO) class of ML models, which have shown efficacy in mapping between function spaces. Following a description by Gopakumar et al. (2024), a NO can be written as a parameterised mapping between function spaces $G_\theta : A \mapsto U$, where G_θ is a neural network parameterised by θ , with three specific architecture elements, which are sequential:

1. **Lifting:** A fully local, point-wise operation that projects the input domain to a higher dimensional latent representation $a \in \mathbb{R}^{d_a} \rightarrow \nu_0 \in \mathbb{R}^{d_{\nu_0}}$,
2. **Iterative Kernel Integration:** Expressed as a sum of a local linear operator, and a non-local integral kernel operator, that iterates $\nu_i \rightarrow \nu_{i+1}$ for several layers:

$$\nu_{i+1} = \sigma(W\nu_i(x) + \kappa(a; \phi)\nu_i(x)),$$

where W is the learnable linear components and σ is a non-linear activation (as in traditional networks). The kernel κ (with learnable parameters ϕ) characterises a neural network’s layer as a convolution, as the following integral with the prior layer’s output ν_i :

$$(\kappa(a; \phi)\nu_i)(x) = \int_D \kappa(x, y, a(x), a(y); \phi)\nu_i(y)dy.$$

3. **Projection** Similar to lifting, but with reversed dimensions $\nu_n \in \mathbb{R}^{d_{\nu_n}} \rightarrow u \in \mathbb{R}^{d_u}$, where n is the total number of layers.

A Fourier Neural Operator is a specific class of the above, which defines κ with Fourier convolutions:

$$(\kappa(a; \phi)\nu_i)(x) = \mathcal{F}^{-1}(\mathcal{F}(R_\phi) \cdot \mathcal{F}(\nu_i)),$$

where \mathcal{F} and \mathcal{F}^{-1} are the Fourier and inverse Fourier transform, and R_ϕ is a learnable complex-valued tensor comprising of truncated Fourier modes. In practical application, the network is discretised to a finite number of modes and the discrete FFT is used for \mathcal{F} . FNOs are learnable using gradient based optimisation using automatic differentiation.

C.3 Training

The trained FNO model consists of

1. **Lifting layer:** a full connected layer $\mathbb{R}^2 \rightarrow \mathbb{R}^{64}$ (192 parameters)
2. **Fourier layers:** 4 Fourier layers (69696 parameters each), each consisting of:
 - (a) a full connected later $\mathbb{R}^{64} \rightarrow \mathbb{R}^{64}$ (4160 parameters)
 - (b) Fourier operator kernel $\mathbb{R}^{64} \rightarrow \mathbb{R}^{64}$, truncated to 16 modes (65536 parameters)
3. **Projection layer:** two layer fully connected network $\mathbb{R}^{64} \rightarrow \mathbb{R}^{125} \rightarrow \mathbb{R}^1$, with Gelu (Gaussian Error Linear Unit) activation (8449 paramaters).

The FNO was trained for 500 epochs using the Adams optimiser with stepsize of 10^{-3} and a weight decay of 10^{-4} , on an L_2 loss, and is timed at around 8 minutes on an NVIDIA A100 GPU.

References

- Canuto, C. (2007). *Spectral Methods: Evolution to Complex Geometries and Applications to Fluid Dynamics*. Springer-Verlag.
- Forets, M. and Schilling, C. (2021). LazySets.jl: Scalable Symbolic-Numeric Set Computations. *Proceedings of the JuliaCon Conferences*, 1(1):11.

- Gopakumar, V., Pamela, S., Zanisi, L., Li, Z., Gray, A., Brennard, D., Bhatia, N., Stathopoulos, G., Kusner, M., Deisenroth, M. P., et al. (2024). Plasma surrogate modelling using Fourier neural operators. *Nuclear Fusion*, 64(5):056025.
- Guibas, L. J., Nguyen, A. T., and Zhang, L. (2003). Zonotopes as bounding volumes. In *SODA*, volume 3, pages 803–812. Citeseer.
- Li, Z., Kovachki, N., Azizzadenesheli, K., Liu, B., Bhattacharya, K., Stuart, A., and Anandkumar, A. (2020). Fourier neural operator for parametric partial differential equations. *arXiv preprint arXiv:2010.08895*.